Applied Catalysis B: Environmental 325 (2023) 122374

Contents lists available at ScienceDirect

Applied Catalysis B: Environmental

journal homepage: www.elsevier.com/locate/apcatb

Inhibitory effect of trace impurities on methanol reforming by Cu/ZnO/Al_2O_3 catalyst: Steam reforming and autothermal reforming of model bio-methanol

Katsutoshi Nomoto [a], Hiroki Miura [a,b,c], Tetsuya Shishido [a,b,c,*]

[a] Department of Applied Chemistry for Environment, Graduate School of Urban Environmental Sciences, Tokyo Metropolitan University, 1–1 Minami-Osawa, Hachioji, Tokyo 192–0397, Japan
[b] Research Center for Hydrogen Energy-based Society, Tokyo Metropolitan University, 1–1 Minami-Osawa, Hachioji, Tokyo 192–0397, Japan
[c] Elements Strategy Initiative for Catalysts and Batteries, Kyoto University, 1–30 Goryo-Ohara, Nishikyo-ku, Kyoto 615–8245, Japan

ARTICLE INFO

Keywords:
Steam reforming
Autothermal reforming
Impurities
Lower alcohols
C-C bond scission
Copper-based catalyst

ABSTRACT

Model bio-methanol was prepared by adding a trace quantity of lower alcohols (ethanol, 1-propanol, and 1-butanol) as model impurities to methanol. The catalytic performance of the Cu/ZnO/Al_2O_3 catalyst for steam reforming (SR) and autothermal reforming (ATR) of model bio-methanol was investigated to evaluate the inhibitory effect of lower alcohols. In SR, the activity (methanol conversion and H_2 production rate) markedly decreased from the initial stage of the reaction. In ATR, the initial activity decreased slightly, and the activity decreased gradually with reaction time. In SR, the lower alcohol adsorbed strongly on the catalyst, resulting in the inhibition of methanol adsorption on Cu. In ATR, although the conversion of lower alcohol was promoted, the quantity of carbonaceous species derived from the lower alcohols increased with the reaction time. These inhibitory effects of lower alcohols were due to the inability of the Cu-based catalyst to cleave C-C bonds in lower alcohols.

1. Introduction

Methanol is an important chemical used industrially as a raw material for various chemical products and fuel. Methanol is also a useful hydrogen carrier that can supply hydrogen to fuel cells on-site because of its several advantages as a hydrogen carrier, including its lower reforming temperature than that of hydrocarbons such as methane and propane, high hydrogen/carbon (H/C) ratio, low soot formation, relatively low boiling point, and easy and safe storage as an aqueous solution at room temperature and atmospheric pressure [1–4]. Therefore, the demand for methanol has continually increased [5,6].

Currently, methanol is mainly produced from fossil fuels such as natural gas and coal. The development of alternative production methods is strongly desired to reduce CO_2 emissions [7] . The alternative methanol production methods include CO_2 hydrogenation [8,9] and converting biomass resources [10–12]. Unlike the biomass-derived ethanol (bio-ethanol) produced by fermentation, biomass-derived methanol (bio-methanol) can be produced from various biomass feedstocks, including inedible lignocellulosic biomass[6,12,13]. In general, bio-methanol contains a trace of impurities including lower alcohols, aromatics, and hydrocarbons[5,6,10–12]. In particular, separating lower alcohols (0–2%) from methanol is challenging and requires energy-intensive purification processes. Establishing the direct utilization of impurity-containing bio-methanol significantly contributes to expanding the use of various biomass resources, reducing costs, and saving energy.

Methanol is used to supply hydrogen to fuel cells on site and the two main reactions are steam reforming (SR, Eq. (1)) [1–3,14–19] and autothermal reforming (oxidative reforming) (ATR, Eq. (2)) [20–22]. Cu-based catalysts are known to exhibit high activity and selectivity for SR and ATR [1–3,15–22].

$$CH_3OH + H_2O \rightarrow 3H_2 + CO_2 \ \Delta H^0_{298} = +\ 49{\cdot}4 \text{ kJ mol}^{-1} \quad (1)$$

Abbreviations: ATR, Autothermal reforming; ESICB, Element Strategy Initiative for Catalysts & Batteries; FID, Flame ionization detector; GC, Gas chromatographs; SR, Steam reforming; TCD, Thermal conductivity detector; TPO, Temperature-programmed oxidation; XRD, X-ray diffraction.

* Corresponding author at: Department of Applied Chemistry for Environment, Graduate School of Urban Environmental Sciences, Tokyo Metropolitan University, 1–1 Minami-Osawa, Hachioji, Tokyo 192–0397, Japan.
E-mail address: shishido-tetsuya@tmu.ac.jp (T. Shishido).

https://doi.org/10.1016/j.apcatb.2023.122374
Received 10 November 2022; Received in revised form 30 December 2022; Accepted 3 January 2023
Available online 6 January 2023

$$CH_3OH + (1-n)\,H_2O + 0{\cdot}5\,n\,O_2 = (3-n)\,H_2 + CO_2\ \Delta H^0_{298} = +49{\cdot}4 - 241{\cdot}6\,n\ \text{kJ mol}^{-1} \quad (2)$$

SR has the advantages of high hydrogen production per CO_2 production and low carbon monoxide (CO) formation; CO poisons the Pt-based electrode catalyst in the fuel cell [1–3] . Although the majority of fuel processing technologies are based on SR, the endothermicity of SR requires continuous external heating of the SR reactor. Indeed, a reaction temperature of 200–300 °C is required to produce hydrogen at a sufficient rate, and SR (Eq. (1)) and partial oxidation (Eq. (3)) can be combined through the simultaneous co-feeding of oxygen, steam, and methanol via autothermal reforming (ATR) [19,23–26].

$$CH_3OH + 0{\cdot}5\,O_2 \rightarrow 2\,H_2 + CO_2\ \Delta H^0_{298} = -192{\cdot}2\ \text{kJ mol}^{-1} \quad (3)$$

In ATR, SR is promoted by the heat generated during the partial oxidation stage. Consequently, the energy input from external sources can be reduced. Moreover, the ATR reactor does not require external heating once it reaches the reaction temperature, because controlling the composition of all three reactants (methanol, water, and oxygen) lowers the overall enthalpy changes of the two reactions to zero.

To date, the effect of impurities on catalyst activity in the SR of ethanol [27] and glycerol [28] has been investigated. The presence of impurities has a negative impact on the catalyst used in SR and ATR. Sulfur compounds and chlorides have been reported to inhibit steam reforming for methanol [29–31]. However, there have been few reports on the effects of lower alcohols which are difficult to separate from methanol on catalytic activity, and the inhibitory effects of lower alcohols on reforming reactions, including the mechanism of inhibition, remain unknown. Ethanol SR proceeds above 300 °C [32–40] because of the necessity for the cleavage of the C-C bonds in the ethanol molecule. Cu-based catalysts are less active in ethanol SR than Ni- and Rh-based catalysts because of their lower C-C bond cleavage ability [41,42]. Cu is also thermally unstable and aggregates at temperatures above 300 °C. Therefore, under the conventional reaction conditions for methanol reforming using a Cu-based catalyst (<300 °C), impurities with C-C bonds are expected to have an inhibitory effect on methanol reforming.

In this study, lower alcohols (ethanol, 1-propanol, and 1-butanol) were added to methanol as model impurities to investigate in detail the effects of impurities on the activity and stability of $Cu/ZnO/Al_2O_3$ (CZA) catalyst for SR and ATR. The mechanism of the inhibitory effect of impurities on the Cu-based catalysts was clarified based on the analysis of impurity-derived byproducts and carbonaceous species deposited during the reaction. This work provides a fundamental understanding of the inhibitory effect of bio-methanol impurities on the catalytic performance in reforming reactions; it provides a strategy for the design of an effective reforming catalyst, which is essential for the direct utilization of bio-methanol.

2. Experimental

2.1. Materials

Copper(II) nitrate trihydrate, zinc(II) nitrate hexahydrate, aluminum (III) nitrate nonahydrate, methanol, 1-propanol, 1-butanol, sodium hydroxide, and sodium carbonate were purchased from FUJIFILM Wako Pure Chemical Corporation (Tokyo, Japan).

2.2. Preparation of catalyst

The CZA catalyst was prepared via a co-precipitation method, i.e., an aqueous solution of the metal nitrates (0.3 M) was added dropwise to an aqueous solution of Na_2CO_3 (0.3 M) with vigorous stirring for 0.5 h, then aged at 50 °C for 20 h [43]. The resulting precipitate was dried at 80 °C for 20 h in an oven and calcined at 300 °C for 3 h. The Cu/Zn/Al molar ratio in the CZA catalyst was 45/45/10.

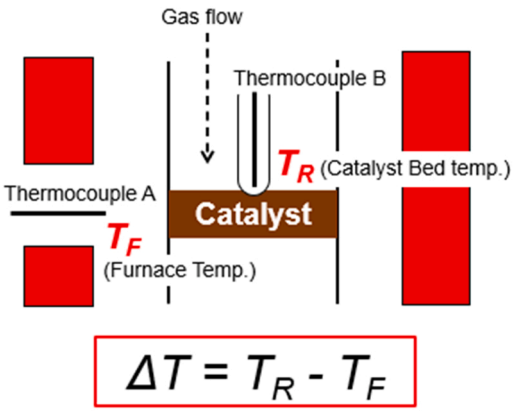

Fig. 1. Furnace Temperature (T_F), Catalysts Bed Temperature (T_R).

2.3. Characterization

X-ray diffraction (XRD) patterns of the catalysts were recorded using a Rigaku SmartLab diffractometer with Cu Kα radiation. The samples were scanned in the 2θ range of 25−50° at a rate of 3° min^{-1} and a resolution of 0.002°.

The temperature-programmed oxidation (TPO) profiles were recorded using a BELCAT II (MicrotracBEL, Osaka, Japan) to determine the quantity of carbonaceous materials deposited during the reaction. Prior to performing the TPO measurements, the spent catalysts were purged at 25 °C for 1 h under He flow (50 mL min^{-1}). Subsequently, the catalysts were heated in 20 vol% O_2 diluted with He at a heating rate of 10 °C min^{-1}. The formation rate of CO_2 ($m/z = 44$) was monitored using a Q-mass (BELMass, MicrotracBEL, Osaka, Japan). The amount of formed CO_2 was quantified using a calibration curve method. The TPO profiles of the catalysts treated with methanol and ethanol were measured. The fresh catalysts were reduced with 16.7 vol% H_2 diluted with He (5/25 mL min^{-1}) at 300 °C for 1 h, and cooled to 40 °C under He flow (30 mL min^{-1}). The pretreated catalyst was thereafter treated with 12 vol% methanol diluted with He or 8 vol% ethanol diluted with He (30 mL min^{-1}) for 1 h, and then flushed with He (30 mL min^{-1}) for 1 h. Subsequently, the catalysts were heated in 20 vol% O_2 diluted with He at a heating rate of 10 °C min^{-1}.

The copper metal surface area was determined according to the N_2O decomposition method using a BELCAT II (MicrotracBEL, Osaka, Japan). Prior to performing this measurement, the sample was reduced at 300 °C for 1 h in a mixed gas flow of H_2 and N_2 (5/25 mL min^{-1}) and cooled to 90 °C under He flow (30 mL min^{-1}). A pulse (1 mL) of 5 vol% N_2O/He was repeatedly introduced into the sample, and the consumption of N_2O was detected by thermal conductivity detector (TCD) and a packed SHINCARBON ST column with He as the carrier gas. As previously reported, a reaction stoichiometry consisting of two Cu atoms per O atom and a Cu surface density of 1.68×10^{19} $Cu_{atoms}\ m^{-2}$ was assumed [44].

Raman spectra of the catalysts were recorded using a NRS-4100R (JASCO, Japan) with a green laser (532.12 nm).

2.4. Catalytic test

SR and ATR of methanol were performed using a fixed-bed flow reactor at atmospheric pressure (Fig. S1). A thermocouple was introduced at the top of the reactor and placed at the top of the catalyst bed to monitor its temperature (T_R). The furnace temperature (T_F) was also measured (Fig. 1), and ΔT was defined as the difference between T_R and T_F. The catalysts were reduced at 300 °C for 1 h under a 14.3 vol% flow of H_2/N_2 (total flow rate: 35 mL min^{-1}). The feed gas compositions were $CH_3OH/H_2O/N_2 = 1.23/1.48/1.23$ mmol min^{-1} (30/36/30 mL min^{-1}) for SR, and $CH_3OH/H_2O/O_2/N_2 = 1.23/1.48/0.41/1.23$ mmol min^{-1} (30/36/10/30 mL min^{-1}) for ATR. The products were analyzed using

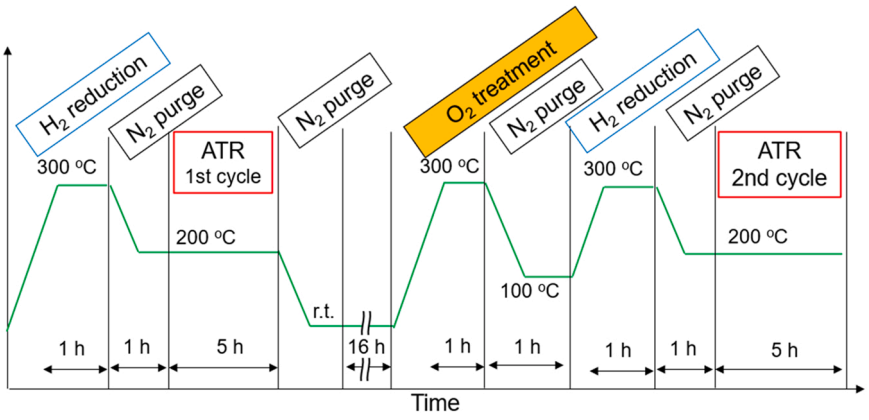

Scheme 1. Procedure of reusability test.

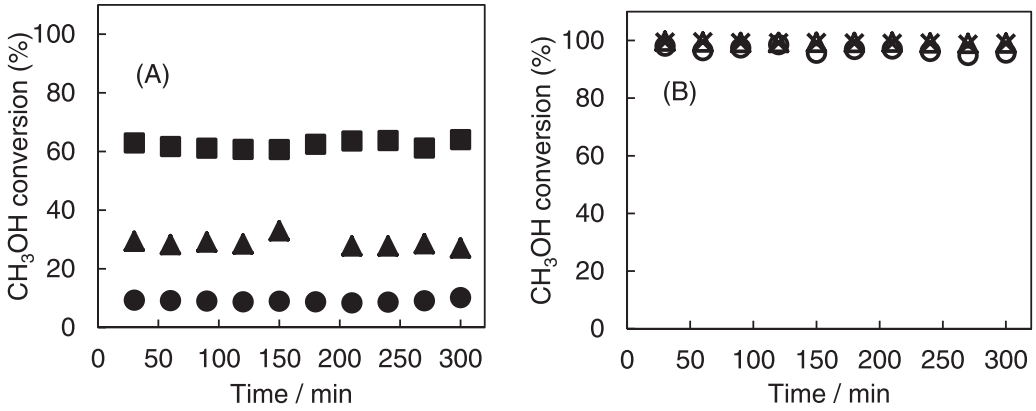

Fig. 2. Time course of methanol conversion in (A) SR and (B) ATR of methanol over CZA catalyst. Reaction conditions: Catalyst 100 mg. SR: T_F (•) 200 °C, (▲) 250 °C, (■) 300 °C; $CH_3OH/H_2O/N_2$ = 1.23/1.48/1.23 mmol min^{-1}. ATR: T_F (◯) 140 °C, (△) 200 °C, (×) 250 °C; $CH_3OH/H_2O/O_2/N_2$ = 1.23/1.48/0.41/1.23 mmol min^{-1}.

two online gas chromatographs (GC). A GC (GC-8A, SHIMADZU, Japan) equipped with a packed Molecular Sieve 5 A column and a TCD was used to analyze H_2 with Ar as the carrier gas. An additional GC (GC-8A, SHIMADZU, Japan) equipped with a Porapak-Q column, a flame ionization detector (FID) and a methanizer (MTN-1, SHIMADZU, Japan) was used to analyze CH_3OH, CH_4, C_2H_4, C_2H_6, CO, and CO_2, with N_2 as the carrier gas. Moreover, the liquid products collected in a cold trap (0 °C) were analyzed by off-line GC (GC-2014, SHIMADZU, Japan) equipped with a DB-FFAP column and a FID.

The conversion of methanol, selectivity to CO, and conversion of ethanol were determined using the following equations:

$$(\text{Methanol conversion})(\%) = \frac{N^{in}_{\text{MeOH}} - N^{out}_{\text{MeOH}}}{N^{in}_{\text{MeOH}}} \times 100 \quad (4)$$

$$(\text{CO selectivity})(\%) = \frac{N^{out}_{\text{CO}}}{N^{out}_{\text{CO2}} + N^{out}_{\text{CO}} + N^{out}_{\text{CH4}}} \times 100 \quad (5)$$

$$(\text{Ethanol conversion})(\%) = \frac{N^{in}_{\text{EtOH}} - N^{out}_{\text{EtOH}}}{N^{in}_{\text{EtOH}}} \times 100 \quad (6)$$

In these equations, N^{in}_{MeOH} and N^{in}_{EtOH} are the initial numbers of moles of methanol and ethanol, N^{out}_{MeOH} and N^{out}_{EtOH} are in the outlet gas of methanol and ethanol, N^{out}_{P} is the number of moles of the product, respectively.

Reusability test was conducted (Scheme 1). After ATR (1st ATR) as described above, the sample was cooled with N_2 (30 mL min^{-1}). Spent catalyst was oxidized at 300 °C under a 25 vol% flow of O_2/N_2 (total flow rate: 40 mL min^{-1}). The sample was cooled to 100 °C flowing N_2

Table 1
Catalytic performance in SR and ATR of methanol over CZA catalyst.

Reforming	T_F /°C	140		200		250		300	
	Time on stream / min	60	300	60	300	60	300	60	300
SR	Methanol conversion (%)	–	–	9.2	10.2	28.3	27.1	61.7	64.1
	Hydrogen production rate / mmol min^{-1}	–	–	0.42	0.41	1.21	1.19	2.37	2.33
	CO concentration (%)	–	–	0.00	0.00	0.01	0.01	0.07	0.07
	ΔT /°C	–	–	-11	-11	-18	-18	-23	-23
ATR	Methanol conversion (%)	96.5	95.7	99.4	99.1	99.5	99.0	–	–
	Hydrogen production rate / mmol min^{-1}	3.02	2.70	3.08	2.89	2.98	2.83	–	–
	CO concentration (%)	0.78	0.72	1.16	1.15	1.45	1.43	–	–
	ΔT /°C	58	62	58	59	44	46	–	–

Reaction conditions: Catalyst 100 mg. SR: $CH_3OH/H_2O/N_2$ = 1.23/1.48/1.23 mmol min^{-1}. ATR: $CH_3OH/H_2O/O_2/N_2$ = 1.23/1.48/0.41/1.23 mmol min^{-1}.

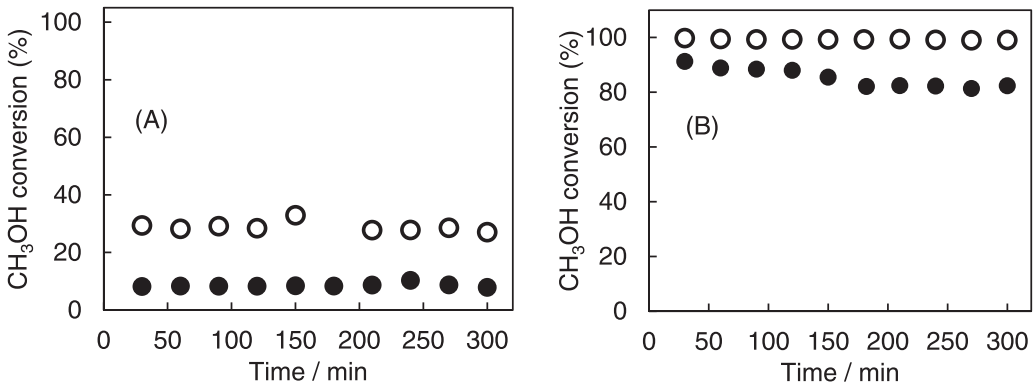

Fig. 3. Time course of methanol conversion in (A) SR and (B) ATR over CZA catalyst. Reaction conditions: Catalyst 100 mg, (○) methanol, (●) model bio-methanol (methanol with 1 mol% ethanol). SR: T_F 250 °C; $CH_3OH/C_2H_5OH/H_2O/N_2$ = 1.23/0.01/1.48/1.23 mmol min^{-1}. ATR: T_F 200 °C; $CH_3OH/C_2H_5OH/H_2O/O_2/N_2$ = 1.23/0.01/1.48/0.41/1.23 mmol min^{-1}.

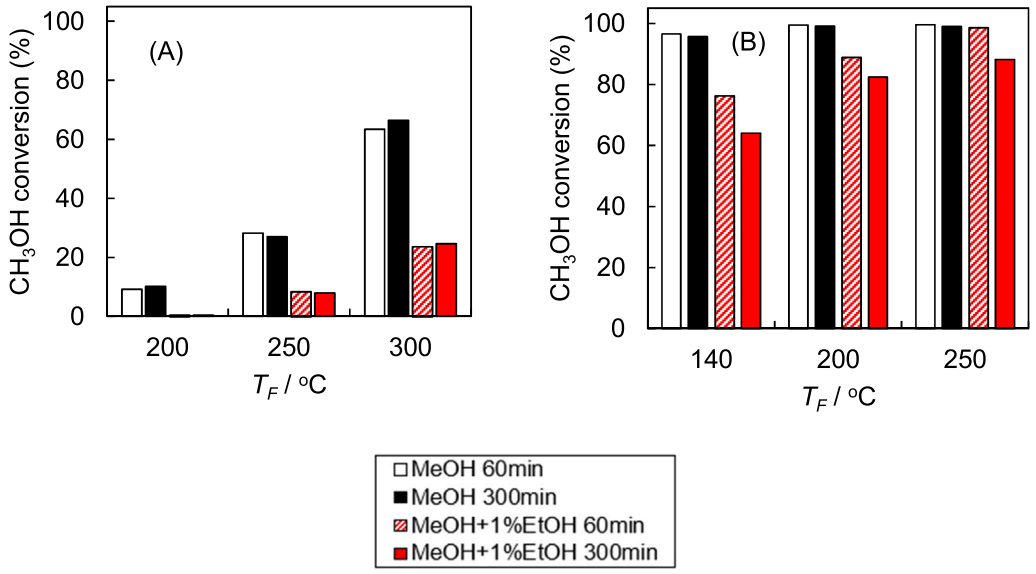

Fig. 4. Effect of temperature (T_F) on catalytic activity in (A) SR and (B) ATR over CZA catalyst. Reaction conditions: Catalyst 100 mg. SR: $CH_3OH/C_2H_5OH/H_2O/N_2$ = 1.23/0.01/1.48/1.23 mmol min^{-1}. ATR: $CH_3OH/C_2H_5OH/H_2O/O_2/N_2$ = 1.23/0.01/1.48/0.41/1.23 mmol min^{-1}.

(30 mL min^{-1}) and then reduced at 300 °C for 1 h under a 14.3 vol% flow of H_2/N_2 (total flow rate: 35 mL min^{-1}). After N_2 treatment, ATR was performed again (2nd ATR).

3. Result and discussion

3.1. Steam reforming and autothermal reforming of methanol

Fig. 2 shows the time course of the conversion of methanol in the SR and ATR of methanol using the CZA catalyst. The CZA catalyst exhibits stable methanol conversion for both SR and ATR reactions, regardless of the reaction temperature. In the SR, the methanol conversion increases with furnace temperature (T_F). In ATR, the methanol conversion is more than 95% at 140 °C (T_F), and the hydrogen production rate reaches 3.0 mmol min^{-1} at the initial stage of the reaction (Table 1.). ΔT is negative for SR, whereas it is positive and large for ATR (Table 1), indicating the progression of the endothermic (SR (Eq. (1))) and exothermic reaction (partial oxidation: PO (Eq. (3))). CO production in the ATR is larger than that in the SR. The large CO production may be due to the contribution of the reverse water gas shift reaction (Eq. (7)) [2,3].

$$CO_2 + H_2 \rightarrow CO + H_2O \ \Delta H^0_{298} = +41{\cdot}0 \text{ kJ mol}^{-1} \quad (7)$$

3.2. Steam reforming and autothermal reforming of model bio-methanol

3.2.1. Catalytic performance

Fig. 3 shows the methanol conversion in SR and ATR of methanol and model bio-methanol (methanol with 1 mol% ethanol) using the CZA catalyst. The furnace temperatures (T_F) were 250 and 200 °C for the SR and ATR, respectively.

In the SR of the model bio-methanol, the methanol conversion is 8.3% after 60 min of reaction, which is much lower than that (28.3%) in the SR of methanol (without ethanol). Methanol conversion is maintained for up to 5 h. In the ATR of the model bio-methanol, the initial methanol conversion is 88.9%, which is slightly lower than that (99.4%) in the ATR of methanol (without ethanol). The methanol conversion gradually decreases with the reaction time and drops to 82.4% after 5 h of the reaction.

The effect of temperature on the inhibitory effect of ethanol was investigated, and methanol conversion after 60 and 300 min at each T_F were compared (Fig. 4). The time course of the methanol conversion is shown in Fig. S2. In the SR, the methanol conversion decreases markedly from the beginning of the reaction at all temperatures tested, upon the

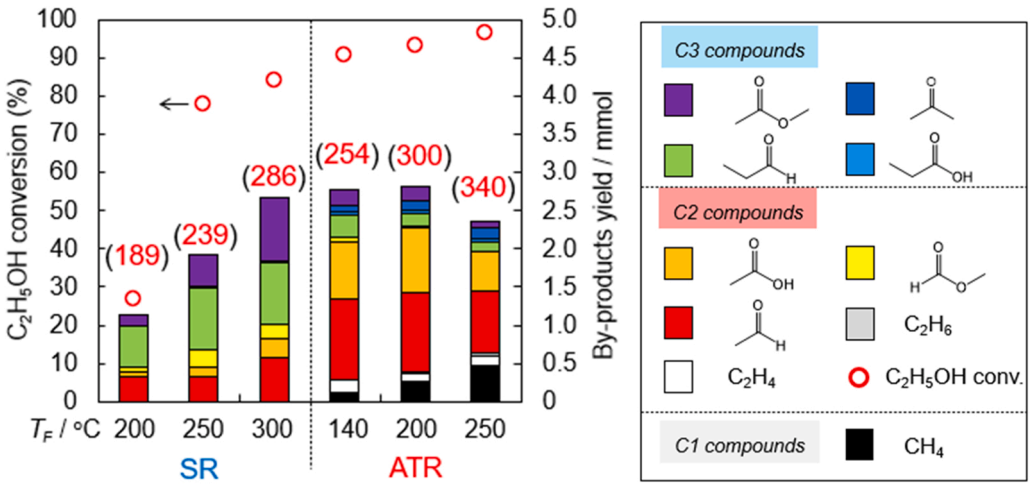

Fig. 5. Yields of byproducts and ethanol conversion in SR and ATR of model bio-methanol over CZA catalyst. Reaction conditions: Catalyst 100 mg, 300 min; the number in parentheses indicate temperature (T_R) of catalyst bed. SR: $CH_3OH/C_2H_5OH/H_2O/N_2$ = 1.23/0.01/1.48/1.23 mmol min^{-1}. ATR: $CH_3OH/C_2H_5OH/H_2O/O_2/N_2$ = 1.23/0.01/1.48/0.41/1.23 mmol min^{-1}.

addition of ethanol. However, the methanol conversion remains stable regardless of the temperature. Furthermore, methanol conversion increases with increasing T_F. In the SR, the ratio of conversion of methanol in bio-methanol reforming ($C_{bio\text{-}MeOH}$) to that in methanol reforming (C_{MeOH}) increases with increasing reaction temperature to 0.05, 0.29, and 0.45 at T_F 200, 250, and 300 °C, respectively. Similar to SR, the $C_{bio\text{-}MeOH}/C_{MeOH}$ ratio increases with increasing T_F in ATR. These results indicate that increasing T_F reduces the inhibitory effect of ethanol.

The yields of the byproducts produced in the SR and ATR of the model bio-methanol (methanol with 1 mol% ethanol) and ethanol conversion are shown in Fig. 5. In both SR and ATR, the ethanol conversion increases with increasing T_F. In SR, C_2 compounds (acetaldehyde, acetic acid, and methyl formate) and C_3 compounds (methyl acetate and propionaldehyde) are formed. The quantity of C_3 compounds is greater than that of C_2 compounds. Acetaldehyde and acetic acid are formed via ethanol dehydrogenation and oxidation, respectively. Methyl formate is an intermediate in methanol SR that forms CO, CO_2, and H_2.

The production rate of acetaldehyde decreases, and that of propionaldehyde increases with increasing contact time (Fig. S3). These results suggest that acetaldehyde is the primary product and propionaldehyde is formed sequentially. In ethanol dehydrogenation, acetone and C_4 compounds (butyraldehyde, ethyl acetate, etc.) have been reported as byproducts of the condensation reaction of acetaldehyde [45]. In the SR of the model bio-methanol, it was assumed that C_3 compounds were generated by condensation of acetaldehyde and methanol-derived C_1 compounds.

In ATR, methane, ethylene, ethane, propionic acid, and acetone are generated in addition to the byproducts produced in the SR. As a result, ATR produces fewer C_3 compounds and more C_2 compounds than did SR. The methane yield in methanol reforming is notably lower than that in bio-methanol reforming (Fig. S4), indicating that the hydrogenation of CO and CO_2 to methane is slow. Therefore, methane is thought to be produced by ethanol decomposition ($C_2H_5OH \rightarrow CH_4 + CO + H_2$) [46–48] and acetaldehyde decomposition ($CH_3CHO \rightarrow CH_4 + CO$). Ethylene and carboxylic acids are thought to be formed by ethanol dehydration ($C_2H_5OH \rightarrow C_2H_4 + H_2O$) [37–40,49] and the oxidation of aldehydes, respectively.

3.2.2. *Characterization of spent catalyst*

In methanol and ethanol reforming, the oxidation and aggregation of copper, and carbon deposition have been proposed as significant reasons

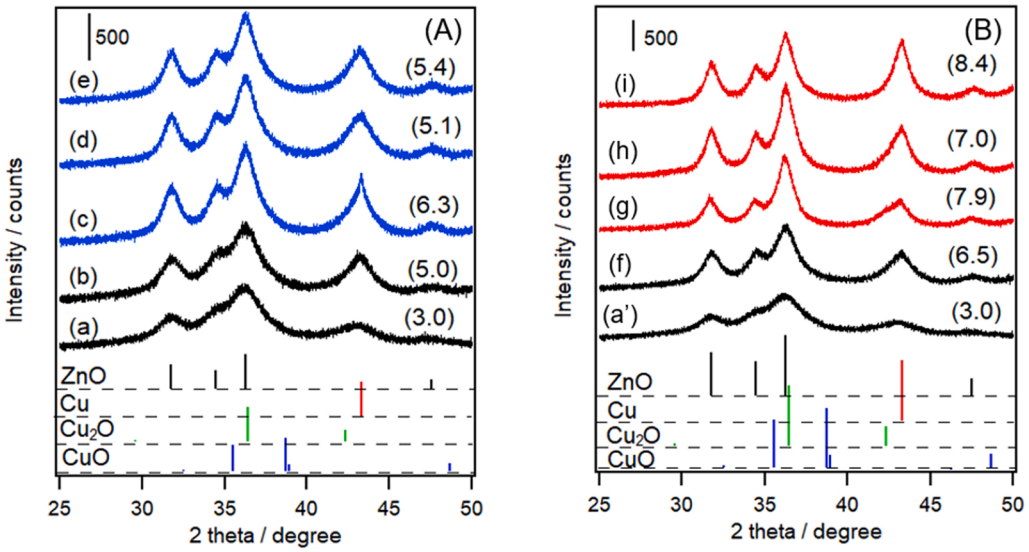

Fig. 6. XRD patterns of spent CZA after (A) SR and (B) ATR of methanol and model bio-methanol (methanol with 1 mol% ethanol), (a, a′) H_2 reduction, (b) methanol at 250 °C, (c) model bio-methanol at 200 °C, (d) model bio-methanol at 250 °C, (e) model bio-methanol at 300 °C, (f) methanol at 200 °C, (g) model bio-methanol at 140 °C, (h) model bio-methanol at 200 °C, and (i) model bio-methanol at 250 °C. Number in parentheses is Cu (111) crystallite diameter (nm), calculated using Scherrer's equation. Reaction conditions: Catalyst 100 mg, 300 min. SR: $CH_3OH/C_2H_5OH/H_2O/N_2$ = 1.23/0.01/1.48/1.23 mmol min^{-1}. ATR: $CH_3OH/C_2H_5OH/H_2O/O_2/N_2$ = 1.23/0.01/1.48/0.41/1.23 mmol min^{-1}.

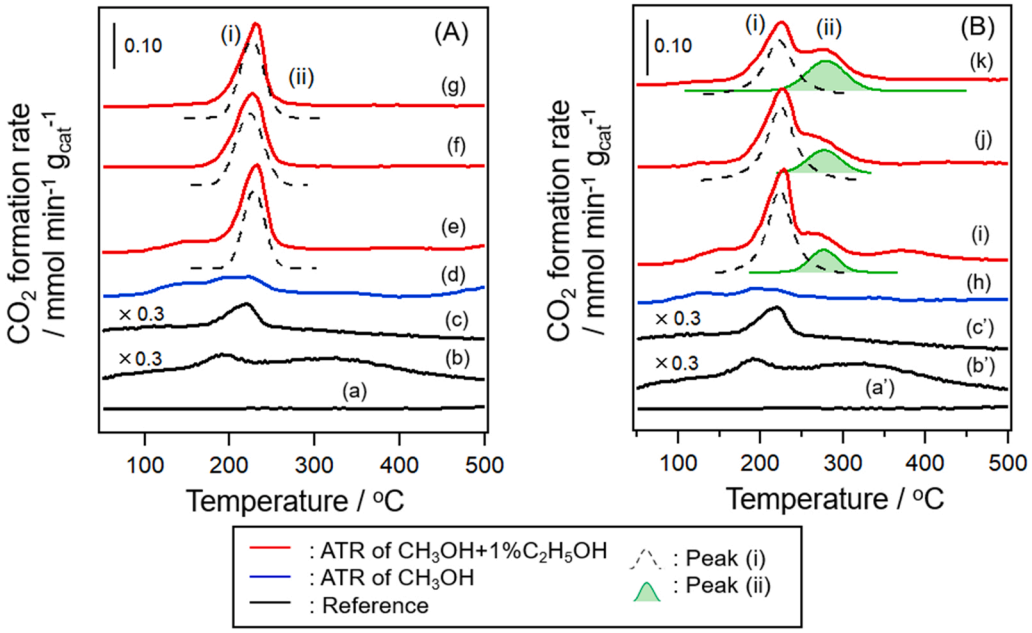

Fig. 7. TPO profiles of spent CZA after (A) SR and (B) ATR of model bio-methanol (methanol with 1 mol% ethanol), (a, a′) after H_2 reduction, (b, b′) methanol adsorption at 40 °C, (c, c′) ethanol adsorption at 40 °C, (d) methanol at 250 °C, (e) model bio-methanol at 200 °C, (f) model bio-methanol at 250 °C, (g) model bio-methanol at 300 °C, (h) methanol at 200 °C, (i) model bio-methanol at 140 °C, (j) model bio-methanol at 200 °C, and (k) model bio-methanol at 250 °C., Reaction conditions: Catalyst 100 mg, 300 min. SR: $CH_3OH(/C_2H_5OH)/H_2O/N_2$ = 1.23 (/0.01)/1.48/1.23 mmol min^{-1}. ATR: $CH_3OH(/C_2H_5OH)/H_2O/O_2/N_2$ = 1.23 (/0.01)/1.48/0.41/1.23 mmol min^{-1}.

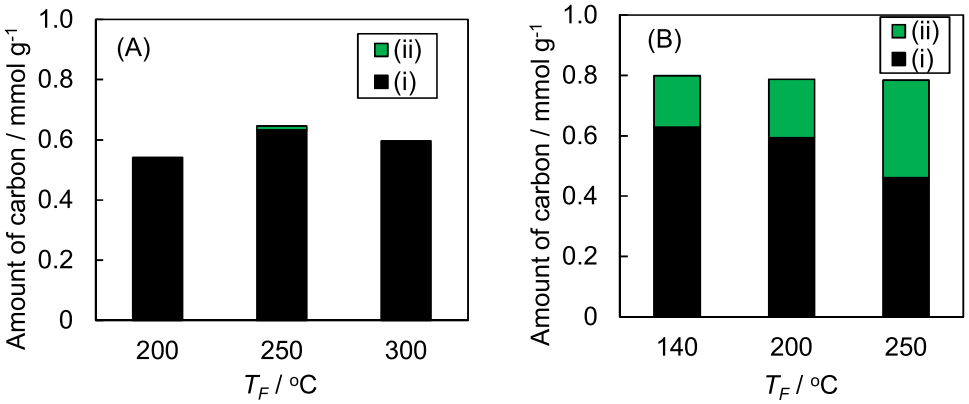

Fig. 8. Amount of carbon formed on spent CZA catalyst after (A) SR and (B) ATR of model bio-methanol (methanol with 1 mol% ethanol), The values ((i) and (ii)) were estimated form the areas of peak (i) and (ii) shown in Fig. 7, Reaction conditions: Catalyst 100 mg, 300 min. SR: $CH_3OH/C_2H_5OH/H_2O/N_2$ = 1.23/0.01/1.48/1.23 mmol min^{-1}. ATR: $CH_3OH/C_2H_5OH/H_2O/O_2/N_2$ = 1.23/0.01/1.48/0.41/1.23 mmol min^{-1}.

for catalyst deactivation [2,37,40]. In ethanol reforming, the formation of carbonaceous species derived from ethylene and acetone reduces the catalytic activity [39,40]. Therefore, we investigated the structural changes and carbon deposition on spent CZA catalysts.

3.2.2.1. XRD. Fig. 6 shows the XRD patterns of the CZA catalyst after the SR and ATR of methanol at various reaction temperatures. In the SR, the Cu crystallite size estimated from the FWHM of the Cu(111) diffraction line does not change. In the ATR, the diffraction peaks due to Cu and ZnO become sharper, suggesting that the aggregation of Cu and ZnO causes catalyst deactivation. Aggregation of Cu and ZnO was also observed after ATR of methanol. The XRD pattern of the CZA catalysts after ATR of the model bio-methanol for 1 h is similar to those for 3 and 5 h (Fig. S5). This result indicates that the aggregation of Cu and ZnO occurred during the initial stage of the reaction. The gradual decrease in methanol conversion with reaction time suggests that Cu and ZnO aggregation is not the primary reason for deactivation.

3.2.2.2. TPO. Fig. 7 shows the TPO profiles of the CZA catalysts after SR and ATR for 5 h. Peak (i) at approximately 220 °C was detected for the spent catalyst after the reforming of model bio-methanol. However, this peak was not observed for the catalyst after the methanol reforming (without ethanol). This temperature (220 °C) is close to the peak observed in the TPO profile of the catalyst treated with ethanol at 40 °C, suggesting that ethanol-derived carbonaceous species are formed on the catalyst surface. Furthermore, the height of peak (i) is maintained even after hydrogen reduction at 300 °C, suggesting that the ethanol-derived carbon species are not removed by treatment with hydrogen (reductive atmosphere) at 300 °C (Fig. S6). Therefore, these carbon species are not removed from the catalyst surface during the SR reaction. Based on these results, we proposed that the decrease in methanol conversion in the SR of bio-methanol is due to poisoning of a part of the metal Cu surface by carbon species derived from lower alcohols.

After ATR, a new peak (ii) was detected at approximately 280 °C. In the case of ATR using methanol or ethanol, peak (ii) was not detected (Fig. S7). In contrast, peak (ii) increases with the reaction time of the ATR of bio-methanol (Fig. S8). This result suggests that carbon deposition is the cause of deactivation. The amount of carbonaceous material formed on the catalyst surface was estimated from the amount of CO_2 produced (Fig. 8). The total amount of carbon (peak (i)+peak (ii)) deposited on the catalyst after 5 h of ATR was higher than that deposited on the catalyst after 5 h of SR. Considering the byproducts formed

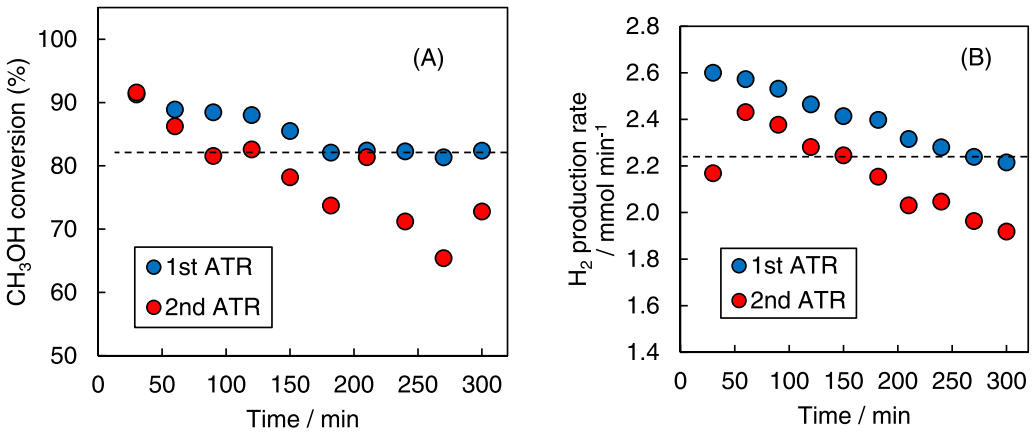

Fig. 9. Time course of (A) methanol conversion and (B) hydrogen production in the reusability test over CZA catalyst. Reaction conditions: Catalyst 100 mg, T_F: 200 °C; $CH_3OH/C_2H_5OH/H_2O/O_2/N_2 = 1.23/0.01/1.48/0.41/1.23$ mmol min^{-1}. The procedure used for the reusability test is shown in Scheme 1.

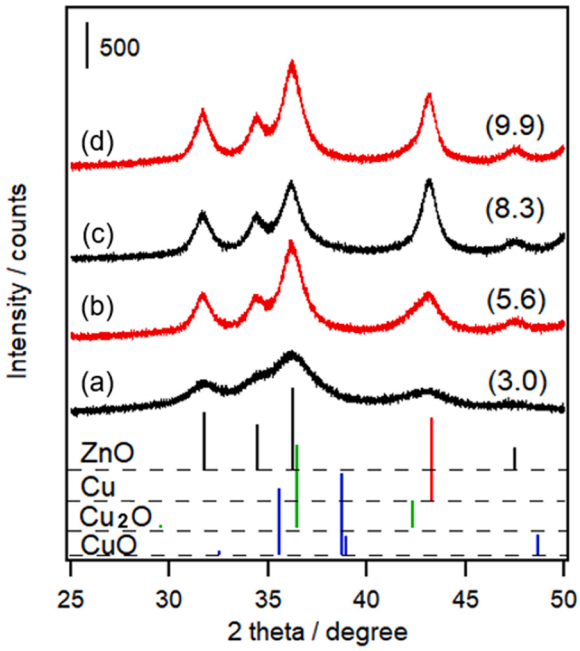

Fig. 10. XRD patterns of CZA before and after the reusability test. (a) after H_2 reduction, (b) after 1st ATR, (c) after O_2 treatment, H_2 reduction, (d) after 2nd ATR, The number in parentheses is the Cu(111) crystallite diameter (nm) calculated using Scherrer's equation. Reaction conditions: Catalyst 100 mg, 300 min, T_F= 200 °C; $CH_3OH/C_2H_5OH/H_2O/O_2/N_2 = 1.23/0.01/1.48/0.41/1.23$ mmol min^{-1}. H_2 reduction: 300 °C, 1 h, $H_2/N_2 = 5/30$ mL min^{-1} , O_2 treatment: 300 °C, 1 h, $O_2/N_2 = 10/30$ mL min^{-1}. The procedure used for the reusability test is shown in Scheme 1.

during ATR, peak (ii) is attributed to the carbonaceous species formed mainly from the byproducts (C_3 compounds). Amount of N_2O adsorption to spent CZA after ATR of the model bio-methanol (methanol with 1 mol % ethanol) (0.095 mmol g_{cat}^{-1}) was remarkably smaller than that after ATR of methanol (0.192 mmol g_{cat}^{-1}) (Table S1). The Cu crystallite size of the spent CZA after ATR of the model bio-methanol (methanol with 1 mol% ethanol) was slightly larger than that after ATR of methanol. This result suggests that carbonaceous species were deposited on spent CZA after ATR of the model bio-methanol. Peaks at approximately 1590 (G Band) and 1350 cm^{-1} (D Band) [40] were not detected in the Raman spectra of the spent catalyst (Fig. S9), indicating that the crystallinity of the carbonaceous species was low.

3.3. Reusability test

Fig. 9 shows the time course of methanol conversion and H_2 production rate for the ATR reusability test (Scheme 1) of the model bio-methanol at 200 °C (T_F). In the 2nd ATR, the initial methanol conversion and H_2 production rate was equal to that of the 1st ATR (fresh catalyst). This result suggests that treatment with oxygen removed the carbon species. The methanol conversion gradually decreased with reaction time in both the 1st and 2nd ATRs. The decrease in activity was attributed to the poisoning of the active site by carbonaceous species. The decrease in methanol conversion in the 2nd ATR was more pronounced than the decrease in methanol conversion in the 1st ATR.

Fig. 10 shows the XRD patterns of the CZA catalysts before and after ATR. The Cu(111) crystallite sizes of the catalysts before the 1st and 2nd ATR were 3.0 and 8.3 nm, respectively. This result suggests that the aggregation of Cu species occurred during ATR and treatment with oxygen to remove the carbon species. Furthermore, the decrease in methanol conversion in the 2nd ATR was more significant than the decrease in methanol conversion in the 1st ATR, suggesting that the decrease in the specific surface area of Cu due to the aggregation of Cu led to more rapidly poisoning by the carbon species.

3.4. Effect of concentration and carbon number of lower alcohols

3.4.1. Effect of carbon number of lower alcohols

The methanol conversions in SR and ATR of model bio-methanols containing ethanol, 1-propanol, and 1-butanol with different carbon numbers as model impurities were compared (Fig. 11). The methanol conversion decreases as the carbon number of the lower alcohols increases for both SR and ATR. In ATR, methanol conversion decreases gradually with reaction time with increasing the chain length of the lower alcohols (Fig. S10). XRD patterns obtained after the reaction (Fig. S11) display no significant structural change regardless of the chain length of the lower alcohols. The size of the Cu crystallites are almost the same for both the lower alcohols added. The TPO profiles of the catalysts after SR and ATR indicate that the peaks at approximately 220 °C and 280 °C become larger as the chain length of the lower alcohols increases, indicating that the amount of carbon increases with increasing chain length of the lower alcohols (Fig. S12).

3.4.2. Effect of concentration of ethanol

Fig. 12 shows the change in the methanol conversion with the ethanol concentration in the SR and ATR of the model bio-methanol. In the SR with 0.1 mol% ethanol, the methanol conversion was about 50% of that without ethanol. However, when 0.1 mol% ethanol was added, the methanol conversion in the initial stage of the reaction was the same

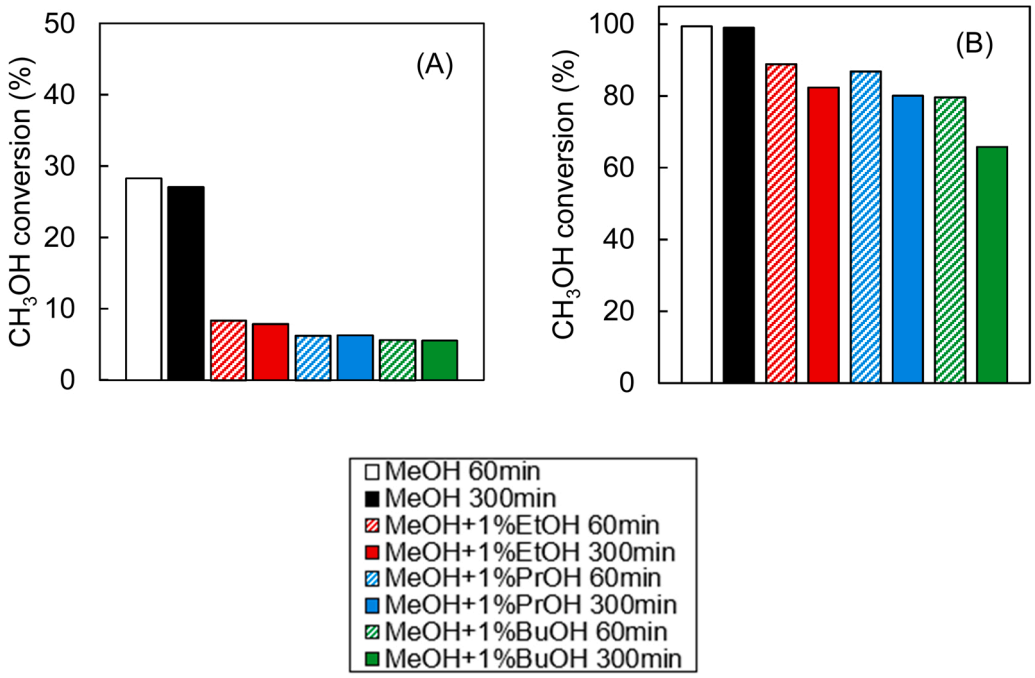

Fig. 11. Time course of methanol conversion in (A) SR and (B) ATR of model bio-methanol (methanol with 1 mol% lower alcohol) over CZA catalyst, Reaction conditions: Catalyst 100 mg. SR: T_F 250 °C; CH_3OH(/Alcohol)/H_2O/N_2 = 1.23(/0.01)/1.48/1.23 mmol min^{-1}, ATR: T_F 200 °C; CH_3OH(/Alcohol)/H_2O/O_2/N_2 = 1.23(/0.01)/1.48/0.41/1.23 mmol min^{-1}.

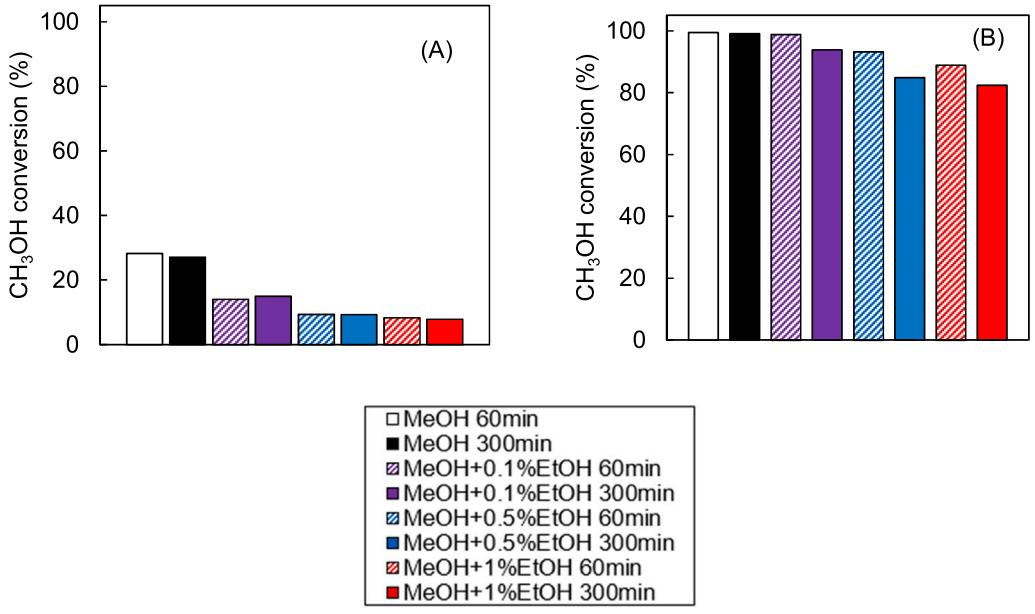

Fig. 12. Effect of ethanol concentration on methanol conversion in (A) SR and (B) ATR over CZA catalyst, Reaction conditions: Catalyst 100 mg. SR: T_F 250 °C; CH_3OH(/C_2H_5OH)/H_2O/N_2 = 1.23(/x)/1.48/1.23 mmol min^{-1}. ATR: T_F 200 °C; CH_3OH(/C_2H_5OH)/H_2O/O_2/N_2 = 1.23(/x)/1.48/0.41/1.23 mmol min^{-1}.

as that without ethanol. In other words, ATR is relatively insensitive to the inhibitory effect of impurities, and is considered an effective way to reduce the inhibitory effect of impurities in the reforming of bio-methanol.

4. Conclusions

In this study, to achieve higher utilization of biomass-derived methanol (bio-methanol), the effect of methanol impurities on the catalytic performance of SR and ATR was investigated. Model bio-methanol was prepared by adding a trace quantity of lower alcohols (ethanol, 1-propanol, and 1-butanol) as model impurities to methanol. The catalytic performance of the $Cu/ZnO/Al_2O_3$ catalyst for SR and ATR of model bio-methanol was investigated to evaluate the inhibitory effect of lower alcohols. For SR, the activity markedly decreased from the initial stage of the reaction because of the strongly adsorbed lower alcohols on the $Cu/ZnO/Al_2O_3$ catalyst, which inhibited the adsorption of methanol on Cu. For ATR, the initial activity decreased slightly, and the activity decreased gradually with time on stream due to carbon deposition derived from lower alcohols. These inhibitory effect of lower alcohols on

the SR and ATR of the model bio-methanol over $Cu/ZnO/Al_2O_3$ catalyst was caused by the inability of Cu to cleave C-C bonds in lower alcohols. This work provides a fundamental understanding of the inhibitory effect of bio-methanol impurities on the catalytic performance of reforming reactions and provides a strategy for the design of an effective reforming catalyst, which is essential for the direct utilization of bio-methanol. Currently, the preparation of a CZA catalyst with C-C bond cleavage ability and its application to reforming reactions of the model bio-methanol are under investigation in our laboratory.

CRediT authorship contribution statement

Katsutoshi Nomoto: Investigation, Methodology, Data curation, Writing - original draft. **Hiroki Miura**: Validation, Writing - review & editing, **Tetsuya Shishido**: Conceptualization, Supervision.

Declaration of Competing Interest

The authors declare that they have no known competing financial interests or personal relationships that could have appeared to influence the work reported in this paper.

Data availability

No data was used for the research described in the article.

Acknowledgments

This study was supported in part by the Program for Element Strategy Initiative for Catalysts & Batteries (ESICB) (Grant JPMXP0112101003), commissioned by MEXT of Japan. In addition, a part of this work was supported by the Tokyo Metropolitan Government Advanced Research Grant Number (R3–1).

Appendix A. Supporting information

Supplementary data associated with this article can be found in the online version at doi:10.1016/j.apcatb.2023.122374.

References

[1] S.T. Yong, C.W. Ooi, S.P. Chai, X.S. Wu, Review of methanol reforming-Cu-based catalysts, surface reaction mechanisms, and reaction schemes, Int. J. Hydrog. Energy 38 (2013) 9541–9552.
[2] S. Sá, H. Silva, L. Brandão, J.M. Sousa, A. Mendes, Catalysts for methanol steam reforming—A review, Appl. Catal. B Environ. 99 (2010) 43–57.
[3] T. Shishido, Y. Yamamoto, H. Morioka, K. Takehira, Production of hydrogen from methanol over Cu/ZnO and Cu/ZnO/Al2O3 catalysts prepared by homogeneous precipitation: Steam reforming and oxidative steam reforming, J. Mol. Catal. Chem. 268 (2007) 185–194.
[4] A. Iulianelli, P. Ribeirinha, A. Mendes, A. Basile, Methanol steam reforming for hydrogen generation via conventional and membrane reactors: A review, Renew. Sustain. Energy Rev. 29 (2014) 355–368.
[5] A. Giuliano, E. Catizzone, D. Barisano, F. Nanna, A. Villone, I. De Bari, G. Cornacchia, G. Braccio, Towards Methanol Economy: A Techno-environmental Assessment for a Bio-methanol OFMSW/Biomass/Carbon Capture-based Integrated Plant, Int. J. Heat. Technol. 37 (2019) 665–674.
[6] N.S. Shamsul, S.K. Kamarudin, N.A. Rahman, N.T. Kofli, An overview on the production of bio-methanol as potential renewable energy, Renew. Sustain. Energy Rev. 33 (2014) 578–588.
[7] G.A. Olah, Beyond Oil and Gas: The Methanol Economy, Angew. Chem. Int. Ed. 44 (2005) 2636–2639.
[8] S.G. Jadhav, P.D. Vaidya, B.M. Bhanage, J.B. Joshi, Catalytic carbon dioxide hydrogenation to methanol: A review of recent studies, Chem. Eng. Res. Des. 92 (2014) 2557–2567.
[9] K. Larmier, W.-C. Liao, S. Tada, E. Lam, R. Verel, A. Bansode, A. Urakawa, A. Comas-Vives, C. Copéret, CO2 -to-Methanol Hydrogenation on Zirconia-Supported Copper Nanoparticles: Reaction Intermediates and the Role of the Metal-Support Interface, Angew. Chem. Int. Ed. 56 (2017) 2318–2323.
[10] Y. Isayama, S. Saka, Biodiesel production by supercritical process with crude bio-methanol prepared by wood gasification, Bioresour. Technol. 99 (2008) 4775–4779.
[11] T. Tsujiguchi, T. Furukawa, N. Nakagawa, Effect of the impurities in crude bio-methanol on the performance of the direct methanol fuel cell, J. Power Sources 196 (2011) 9339–9345.
[12] P. Gautam, Neha, S.N. Upadhyay, S.K. Dubey, Bio-methanol as a renewable fuel from waste biomass: Current trends and future perspective, Fuel 273 (2020), 117783.
[13] C.N. Hamelinck, A.P.C. Faaij, Future prospects for production of methanol and hydrogen from biomass, J. Power Sources 111 (2002) 22.
[14] D.L. Trimm, Z.I. Önsan, Onboard Fuel Conversion for Hydrogen-Fuel-Cell-Driven Vehicles, Catal. Rev. 43 (2001) 31–84.
[15] J.P. Breen, J.R.H. Ross, Methanol reforming for fuel-cell applications: development of zirconia-containing Cu–Zn–Al catalysts, Catal. Today 51 (1999) 521–533.
[16] X. Huang, L. Ma, M.S. Wainwright, The influence of Cr, Zn and Co additives on the performance of skeletal copper catalysts for methanol synthesis and related reactions, Appl. Catal. Gen. 257 (2004) 235–243.
[17] Y. Liu, T. Hayakawa, T. Tsunoda, K. Suzuki, S. Hamakawa, K. Murata, R. Shiozaki, T. Ishii, M. Kumagai, Top. Catal. 22 (2003) 205–213.
[18] S. Patel, K.K. Pant, Activity and stability enhancement of copper–alumina catalysts using cerium and zinc promoters for the selective production of hydrogen via steam reforming of methanol, J. Power Sources 159 (2006) 139–143.
[19] S. Lin, D. Xie, H. Guo, Pathways of Methanol Steam Reforming on PdZn and Comparison with Cu, J. Phys. Chem. C. 115 (2011) 20583–20589.
[20] S. Velu, K. Suzuki, M.P. Kapoor, F. Ohashi, T. Osaki, Selective production of hydrogen for fuel cells via oxidative steam reforming of methanol over CuZnAl(Zr)-oxide catalysts, Appl. Catal. Gen. 213 (2001) 47–63.
[21] M. Turco, G. Bagnasco, U. Costantino, F. Marmottini, T. Montanari, G. Ramis, G. Busca, Production of hydrogen from oxidative steam reforming of methanol I. Preparation and characterization of Cu/ZnO/Al2O3 catalysts from a hydrotalcite-like LDH precursor, J. Catal. 228 (2004) 43–55.
[22] M. Turco, G. Bagnasco, U. Costantino, F. Marmottini, T. Montanari, G. Ramis, G. Busca, Production of hydrogen from oxidative steam reforming of methanol II. Catalytic activity and reaction mechanism on Cu/ZnO/Al2O3 hydrotalcite-derived catalysts, J. Catal. 228 (2004) 56–65.
[23] L. Alejo, R. Lago, M.A. Peña, J.L.G. Fierro, Partial oxidation of methanol to produce hydrogen over Cu-Zn-based catalysts, Appl. Catal. Gen. 162 (1997) 281–297.
[24] J. Agrell, M. Boutonnet, I. Melián-Cabrera, J.L.G. Fierro, Production of hydrogen from methanol over binary Cu/ZnO catalysts: Part I. Catalyst preparation and characterisation, Appl. Catal. Gen. 253 (2003) 201–211.
[25] T.B. Rawal, S.R. Acharya, S. Hong, D. Le, Y. Tang, F.F. Tao, T.S. Rahman, High Catalytic Activity of Pd1/ZnO(10$\bar{1}$0) toward Methanol Partial Oxidation: A DFT+KMC Study, ACS Catal. 8 (2018) 5553–5569.
[26] Z.-J. Zuo, X.-Y. Gao, P.-D. Han, S.-Z. Liu, W. Huang, Density Functional Theory (DFT) and Kinetic Monte Carlo (KMC) Study of the Reaction Mechanism of Hydrogen Production from Methanol on ZnCu(111), J. Phys. Chem. C. 120 (2016) 27500–27508.
[27] A. Le Valant, F. Can, N. Bion, D. Duprez, F. Epron, Hydrogen production from raw bioethanol steam reforming: Optimization of catalyst composition with improved stability against various impurities, Int. J. Hydrog. Energy 35 (2010) 5015–5020.
[28] K. Wu, B. Dou, H. Zhang, D. Liu, H. Chen, Y. Xu, Effect of impurities of CH3OH, CH3COOH, and KOH on aqueous phase reforming of glycerol over mesoporous Ni–Cu/CeO2 catalyst, J. Energy Inst. 99 (2021) 198–208.
[29] M.V. Twigg, M.S. Spencer, Deactivation of supported copper metal catalysts for hydrogenation reactions, Appl. Catal. Gen. 212 (2001) 161–174.
[30] M.V. Twigg, M.S. Spencer, Deactivation of copper metal catalysts for methanol decomposition, methanol steam reforming and methanol synthesis, Top. Catal. 22 (2003) 191–203.
[31] H. Yoon, P. Erickson, Hydrogen from coal-derived methanol via autothermal reforming processes, Int. J. Hydrog. Energy 33 (2008) 57–63.
[32] D.K. Liguras, D.I. Kondarides, X.E. Verykios, Production of hydrogen for fuel cells by steam reforming of ethanol over supported noble metal catalysts, Appl. Catal. B Environ. 43 (2003) 345–354.
[33] A. Fatsikostas, Reaction network of steam reforming of ethanol over Ni-based catalysts, J. Catal. 225 (2004) 439–452.
[34] N. Homs, J. Llorca, P.R. de la Piscina, Low-temperature steam-reforming of ethanol over ZnO-supported Ni and Cu catalysts, Catal. Today 116 (2006) 361–366.
[35] G.A. Deluga, Renewable Hydrogen from Ethanol by Autothermal Reforming, Science 303 (2004) 993–997.
[36] E. Finocchio, I. Rossetti, G. Ramis, Redox properties of Co- and Cu-based catalysts for the steam reforming of ethanol, Int. J. Hydrog. Energy 38 (2013) 3213–3225.
[37] L.V. Mattos, G. Jacobs, B.H. Davis, F.B. Noronha, Production of Hydrogen from Ethanol: Review of Reaction Mechanism and Catalyst Deactivation, Chem. Rev. 112 (2012) 4094–4123.
[38] J.L. Contreras, J. Salmones, J.A. Colín-Luna, L. Nuño, B. Quintana, I. Córdova, B. Zeifert, C. Tapia, G.A. Fuentes, Catalysts for H2 production using the ethanol steam reforming (a review), Int. J. Hydrog. Energy 39 (2014) 18835–18853.
[39] T. Hou, S. Zhang, Y. Chen, D. Wang, W. Cai, Hydrogen production from ethanol reforming: Catalysts and reaction mechanism, Renew. Sustain. Energy Rev. 44 (2015) 132–148.
[40] Y.C. Sharma, A. Kumar, R. Prasad, S.N. Upadhyay, Ethanol steam reforming for hydrogen production: Latest and effective catalyst modification strategies to minimize carbonaceous deactivation, Renew. Sustain. Energy Rev. 74 (2017) 89–103.
[41] D.K. Liguras, D.I. Kondarides, X.E. Verykios, Production of hydrogen for fuel cells by steam reforming of ethanol over supported noble metal catalysts, Appl. Catal. B Environ. 43 (2003) 345–354.

[42] S. Ogo, Y. Sekine, Recent progress in ethanol steam reforming using non-noble transition metal catalysts: A review, Fuel Process. Technol. 199 (2020), 106238.
[43] T. Shishido, Y. Yamamoto, H. Morioka, K. Takaki, K. Takehira, Active Cu/ZnO and Cu/ZnO/Al2O3 catalysts prepared by homogeneous precipitation method in steam reforming of methanol, Appl. Catal. Gen. 263 (2004) 249–253.
[44] J.W. Evans, M.S. Wainwright, A.J. Bridgewater, D.J. Young, On the determination of copper surface area by reaction with nitrous oxide, Appl. Catal. 7 (1983) 75–83.
[45] K. Inui, T. Kurabayashi, S. Sato, N. Ichikawa, Effective formation of ethyl acetate from ethanol over Cu-Zn-Zr-Al-O catalyst, J. Mol. Catal. Chem. 216 (2004) 147–156.
[46] G. Carotenuto, A. Kumar, J. Miller, A. Mukasyan, E. Santacesaria, E.E. Wolf, Hydrogen production by ethanol decomposition and partial oxidation over copper/copper-chromite based catalysts prepared by combustion synthesis, Catal. Today 203 (2013) 163–175.
[47] K.V. Manukyan, A.J. Cross, A.V. Yeghishyan, S. Rouvimov, J.J. Miller, A. S. Mukasyan, E.E. Wolf, Highly stable Ni–Al2O3 catalyst prepared from a Ni–Al layered double hydroxide for ethanol decomposition toward hydrogen, Appl. Catal. Gen. 508 (2015) 37–44.
[48] M.A. Goula, S.K. Kontou, P.E. Tsiakaras, Hydrogen production by ethanol steam reforming over a commercial Pd/γ-Al2O3 catalyst, Appl. Catal. B Environ. 49 (2004) 135–145.
[49] I. Takahara, M. Saito, M. Inaba, K. Murata, Dehydration of ethanol into ethylene over solid acid catalysts, Catal. Lett. 105 (2005) 249–252.